Improved correction of B_0 inhomogeneity-induced distortions in diffusion-weighted images of the prostate

Christopher C Conlin, PhD[1], Aditya Bagrodia, MD[2], Tristan Barrett, MD[3], Madison T Baxter, MS[4], Deondre D Do, BS[4,5], Michael E Hahn, MD, PhD[1], Mukesh G Harisinghani, MD[6], Juan F Javier-DesLoges, MD[2], Karoline Kallis, PhD[4], Christopher J Kane, MD[2], Joshua M Kuperman, PhD[1], Michael A Liss, MD, PhD[7], Daniel JA Margolis, MD[8], Paul M Murphy, MD, PhD[1], Michael Ohliger, MD, PhD[9], Courtney Ollison, BS[4], Rebecca Rakow-Penner, MD, PhD[1], Mariluz Rojo Domingo, MS[4,5], Yuze Song, MS[4,10], Natasha Wehrli, MD[8], Sean Woolen, MD[9], Tyler M Seibert, MD, PhD[1,4,5], Anders M Dale, PhD[1,11,12]

[1]Department of Radiology, University of California San Diego School of Medicine, La Jolla, CA, USA
[2]Department of Urology, University of California San Diego School of Medicine, La Jolla, CA, USA
[3]Department of Radiology, Addenbrooke's Hospital, Cambridge University Hospitals NHS Foundation Trust, Cambridge, UK
[4]Department of Radiation Medicine and Applied Sciences, University of California San Diego School of Medicine, La Jolla, CA, USA
[5]Department of Bioengineering, University of California San Diego Jacobs School of Engineering, La Jolla, CA, USA
[6]Department of Radiology, Massachusetts General Hospital, Boston, MA, USA
[7]Department of Urology, University of Texas Health San Antonio, San Antonio, TX, USA
[8]Department of Radiology, Weill Cornell Medicine, New York, NY, USA
[9]Department of Radiology and Biomedical Imaging, University of California San Francisco, San Francisco, CA, USA
[10]Department of Electrical and Computer Engineering, University of California San Diego Jacobs School of Engineering, La Jolla, CA, USA
[11]Department of Neurosciences, University of California San Diego School of Medicine, La Jolla, CA, USA
[12]Halıcıoğlu Data Science Institute, University of California San Diego, La Jolla, CA, USA

Abstract

Background: Conventional distortion correction techniques include the Reversed Polarity Gradient (RPG) method and FSL-topup, which estimate tissue displacement from EPI images of opposite phase-encoding polarity, and scale image intensity by the Jacobian of the estimated displacement.

Purpose: To demonstrate that Jacobian intensity correction (JIC) can cause misleading improvement of EPI image distortion. We propose an alternative distortion correction approach (multi-*b* RPG; mRPG) that eliminates the JIC factor by normalizing opposite-polarity EPI images across multiple *b*-values.

Study type: Retrospective.

Population: 163 prostate cancer patients without metallic implants.

Fieldstrength/Sequence: 3T diffusion-weighted sequence with EPI readout, using multiple *b*-values.

Assessment: Maps of spatial shift (distortion) were estimated from opposite-polarity EPI volumes using RPG, topup, and mRPG. The estimated spatial shifts from each method were then applied to correct the b=0s/mm^2 images (both with and without JIC) and ADC maps (for which JIC is meaningless).

Distortion was quantified by the Pearson correlation between opposite-polarity volumes. The distribution of correlation coefficients across all patients was examined for b=0s/mm^2 images and ADC maps, before and after distortion correction by each method. The mean, median, and 10th percentile were reported for each distribution.

Statistical tests: Wilcoxon signed-rank tests (α=0.05) were used to assess whether correlation increased significantly after distortion correction by each method, and whether mRPG yielded a larger increase versus RPG or topup.

Results: Median improvement in the correlation between b=0s/mm^2 volumes was significantly smaller without JIC ($p<0.001$): 0.04 vs 0.16 (RPG), 0.06 vs 0.18 (topup). mRPG yielded significantly larger improvements compared to RPG or topup ($p<0.001$). b=0s/mm^2: 0.09 vs 0.04 (RPG) and 0.06 (topup). ADC: 0.09 vs 0.02 (RPG) and 0.03 (topup).

Data conclusion: Disparity in the distortion-correction performance of conventional methods with and without JIC suggests underestimation of tissue displacement. mRPG shows improved correction of distortion artifacts compared to conventional methods.

Introduction

Diffusion-weighted imaging (DWI) is an important technique for identifying tumors in patients with suspected prostate cancer. In addition to its longstanding diagnostic utility as part of the Prostate Imaging Reporting and Data System (PI-RADS) (1), DWI has recently proven to be a valuable aid for accurately targeting prostate tumors with radiation therapy (2). However, DWI data acquired with standard echo-planar imaging (EPI) trajectories are prone to distortion artifacts that arise from inhomogeneities in the static magnetic field (B_0). These artifacts present as compression or expansion of tissue in the phase-encoding direction, with compressed regions displaying increased signal intensity from the additional spins incorrectly localized to each voxel. Conversely, expanded regions show reduced signal intensity from the apparent decrease in spins within each voxel. The tissue-air interface where the prostate meets the rectum often causes considerable distortion of the local anatomy, which may obscure the precise location of a lesion and limits the ability to perform targeted biopsy or therapy (3).

A common approach to correct for such distortion involves the acquisition of two EPI images, typically without diffusion weighting (i.e., b=0 s/mm^2), and with opposite phase-encoding polarity. These images will necessarily show opposing distortion artifacts, with tissue compression in one image and expansion in the other. By estimating the spatial displacements and associated signal intensity changes between the two images, the distortions can be undone. Techniques utilizing this approach include the Reversed Polarity Gradient (RPG) method (3, 4) and FSL-topup (5, 6), which simultaneously estimate the spatial and signal-intensity aspects of distortion, with intensities scaled by the Jacobian of the estimated tissue displacement. Here the Jacobian refers to the partial derivative of tissue displacement along the phase-encoding direction, which quantifies the amount of local compression or expansion of tissue and the resulting concentration or dilution of signal intensity in the acquired image.

In this study, we demonstrate that this Jacobian intensity correction (JIC) can result in misleading improvement of EPI image distortion and even create false anatomical structure in DWI images of the prostate. We propose an alternative method for correcting EPI distortions that avoids these issues by removing the intensity scaling factor prior to estimating spatial displacement, specifically by normalizing the opposed-phase images across multiple *b*-values.

Materials and Methods

This study was approved by the Institutional Review Board (IRB). Patients were considered for this study if they underwent supplemental DWI for suspected or biopsy-proven prostate cancer between March and October of 2023, and were excluded if they had metal hip implants or other devices that caused severe EPI-distortion artifacts.

MRI acquisition and pre-processing

All MR imaging was performed on 3T clinical scanners (SIGNA Premier; GE Healthcare), using a 32-channel phased-array body coil placed over the pelvis. Two axial, multi-*b*-value DWI volumes were acquired per patient, using EPI readouts with opposite phase-encoding polarity along the anterior-posterior axis (arbitrarily referred to as “forward” and “reverse” volumes hereafter). The two volumes were otherwise identical. Water-selective excitation pulses were used for fat suppression. High resolution T_2-weighted volumes without fat suppression were also acquired for anatomical reference. This protocol was developed to support advanced quantitative DWI (2, 7–9) and is currently in clinical use at our center, as well as part of a prospective, multi-center, international trial. Acquisition parameters are summarized in Table 1.

	Acquisition time (min:sec)	b-values (s/mm^2) [number of samples]	FOV (mm)	Matrix	Slices	Slice thickness (mm)	TR (ms)	TE (ms)
DWI	3:25	0 [4], 100 [6], 800 [12], 1400 [12], 2500 [18]	200×200	80×80	32	3	4500	80
T2W	2:07	N/A	200×200	452×300	32	3	5600	170

Table 1: MRI acquisition details for the patients included in this study. Two axial DWI volumes were acquired per patient using the same diffusion-weighted spin-echo pulse sequence (default tensor), but with EPI readout trajectories of opposite phase-encoding polarity along the anterior-posterior axis. Water-selective excitation pulses were used for fat signal suppression. The high-resolution T_2-weighted (T2W) volume was acquired for anatomical reference using a fast spin-echo (FSE) pulse sequence without fat suppression.

Image processing and data analysis was performed using custom programs written in MATLAB (The MathWorks, Inc). DWI samples acquired at each *b*-value were first averaged together. ADC maps were then computed from the averaged forward- and reverse-polarity DWI volumes by fitting the signal from *b*-values less than 1000 s/mm^2 with a monoexponential decay model.

Proposed distortion correction method (multi-*b* RPG)

The forward and reverse DWI volumes were first normalized by their sum across all *b*-values. Normalizing the DWI volumes across *b*-values eliminates the intensity changes resulting from tissue compression or expansion (see Figure 1B), obviating the need to fit a Jacobian term when attempting to identify corresponding locations for each voxel in forward and reverse images. Estimating spatial displacements between the images is then reduced to a much simpler image registration problem, for which any suitable algorithm may be used. In this study, registration was performed by shifting the forward and reverse volumes along the anterior-posterior axis and computing the amount of shift for each voxel that minimizes the difference

between forward and reverse images. This approach amounts to a multi-*b*-value adaptation of RPG, so we call it multi-*b* RPG (mRPG).

Figure 1 shows an example application of the proposed mRPG method to correct EPI distortion of prostate diffusion data. Prior to correction, the posterior prostate (abutting the rectum) is stretched in the forward image and compressed in the reverse, relative to the undistorted anatomy in the reference spin echo image. Signal enhancement of compressed tissue is readily apparent along the posterior edge of the prostate in the reverse b=0 s/mm^2 image. Following correction by mRPG, the posterior edge of the prostate in the diffusion images matches that of the undistorted reference image.

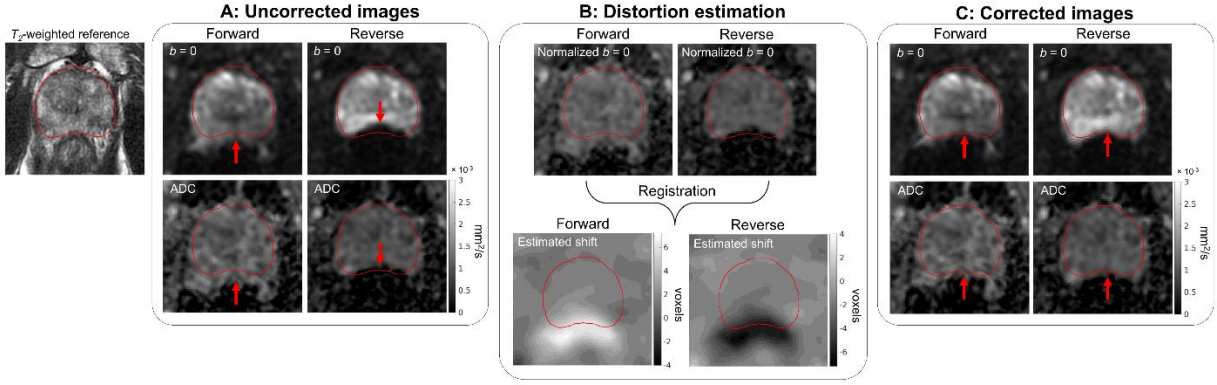

Figure 1: Example of mRPG distortion correction. An undistorted spin echo (T_2-weighted) image is shown on the left, with the prostate outlined in red. A) Uncorrected diffusion data, with stretching of the posterior prostate in the forward direction and compression in the reverse (arrows). B) Registration of the normalized forward- and reverse-images yields the estimated voxel shifts. C) Corrected images after application of the shift maps in B, with reduced spatial distortion (arrows).

Application of distortion correction methods

For each patient, maps of spatial shift (in units of voxels) were estimated from the forward- and reverse-polarity EPI volumes using RPG, topup, and mRPG. RPG software was provided by request from the developers of the algorithm (4). Topup was obtained as part of the FMRIB Software Library (FSL) (10) version 5.0.2.2, compiled for 64-bit CentOS 6. For both RPG and topup, shift maps were estimated from the b=0 s/mm^2 volumes as outlined in prior studies, according to the documentation provided with each software package (4–6). The estimated spatial shifts from each method were then applied to correct the b=0 s/mm^2 images and ADC maps. For RPG and topup, a second correction incorporating the JIC was applied to the b=0 s/mm^2 images (JIC is meaningless for quantitative ADC values).

Statistical analysis

Statistical analyses were performed using MATLAB. EPI distortion was quantified by the Pearson correlation coefficient between the forward and reverse volumes. The distribution of correlation coefficients across all patients was examined for b=0 s/mm^2 images and ADC maps, before and after distortion correction by each method. The distributions were visualized using violin plots (11, 12), and the mean, median, and 10th percentile were reported for each distribution. The 10th percentile was chosen to quantify the severity of distortion in patients most impacted by B_0-inhomogeneity artifacts, having the lowest correlation between forward and reverse volumes. Wilcoxon signed-rank tests (α=0.05) were used to assess whether the

Pearson correlation increased significantly after distortion correction by each method, and whether mRPG yielded a larger increase in correlation compared to RPG or topup.

Results

In total, 175 consecutive patients were considered for this study. Twelve were excluded due to the presence of implanted metallic devices, leaving 163 patients for analysis.

The violin plots in Figure 2 show the distribution across patients of the Pearson correlation between opposite-polarity diffusion volumes. Point estimates for the mean, median, and 10th percentile of each distribution are listed in Table 2. With JIC applied, both RPG and topup yielded a considerable increase in correlation between forward and reverse b=0 s/mm^2 acquisitions. The median correlation increased from 0.80 before correction, to 0.96 after correction with RPG and 0.98 after correction with topup. The 10th percentile improved from 0.64 before correction, to 0.84 after correction with RPG and 0.96 after correction with topup.

When the estimated spatial corrections were applied without the JIC, the observed increase in correlation was much smaller (albeit still statistically significant). The median correlation between b=0 s/mm^2 volumes increased from 0.80 before correction to 0.84 using RPG and 0.86 using topup. The 10th percentile increased from 0.64 before correction to 0.66 using RPG and decreased to 0.62 using topup. The median correlation between ADC maps increased from 0.72 before correction to 0.74 using RPG and 0.75 using topup. The 10th percentile improved from 0.62 before correction, to 0.65 using RPG and 0.64 using topup.

Spatial corrections estimated using the proposed mRPG approach yielded a substantial improvement in correlation compared to either RPG or topup. The median correlation between forward and reverse b=0 s/mm^2 acquisitions increased to 0.89 using mRPG, versus 0.84 using RPG and 0.86 using topup. The 10th percentile increased to 0.80 using mRPG, versus 0.66 using RPG and 0.62 using topup. The median correlation between ADC maps increased to 0.81 using mRPG, versus 0.74 using RPG and 0.75 using topup. The 10th percentile increased to 0.76 using mRPG, versus 0.65 using RPG and 0.64 using topup.

Notably, application of the JIC concealed poor estimation of tissue displacement, as illustrated by the example images in Figure 3. While the uncorrected diffusion images from this patient showed minimal EPI distortion, RPG estimated large shifts in the posterior prostate. When the estimated spatial correction is applied without the JIC, the overcorrection is readily apparent. Application of the JIC obscured the overcorrection, however, adjusting image intensity to yield an apparent alignment of the posterior prostate between the EPI images and the reference spin echo image. Furthermore, the JIC resulted in false anatomical structure or “ghost tissue” between the posterior prostate and rectum. mRPG, by contrast, yielded appropriate spatial correction for this patient.

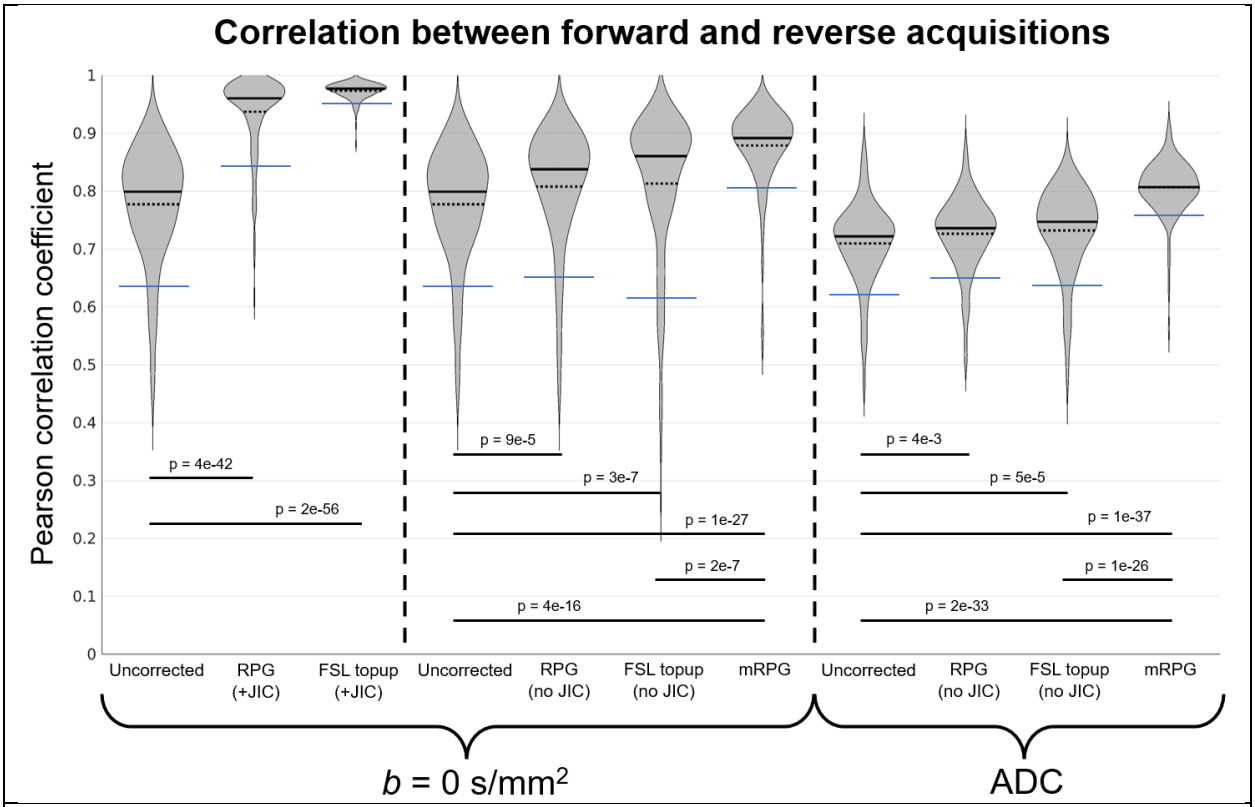

Figure 2: Improved correlation between opposite-polarity diffusion volumes before and after EPI-distortion correction. The 10th percentile, mean, and median of each distribution is indicated by the blue line, dashed black line, and solid black line, respectively. RPG and topup considerably increased the correlation of b=0 s/mm^2 images when the Jacobian intensity correction (JIC) was applied. Without the JIC, however, both RPG and topup yielded much smaller increases than mRPG, suggesting an underestimation of tissue displacement.

	b = 0 s/mm^2						ADC			
	Uncorrected	RPG (no JIC)	RPG (+JIC)	FSL topup (no JIC)	FSL topup (+JIC)	mRPG	Uncorrected	RPG (no JIC)	FSL topup (no JIC)	mRPG
10th percentile	0.64	0.66	0.84	0.62	0.96	0.80	0.62	0.65	0.64	0.76
Median	0.80	0.84	0.96	0.86	0.98	0.89	0.72	0.74	0.75	0.81
Mean	0.78	0.81	0.94	0.81	0.97	0.88	0.71	0.73	0.73	0.81

Table 2: Point estimates for the distributions of correlation coefficients shown in Figure 2. RPG and topup show high correlation values for b=0 s/mm^2 images when the JIC is applied, but without the JIC yield much lower correlation values than mRPG for either b=0 s/mm^2 images or ADC maps.

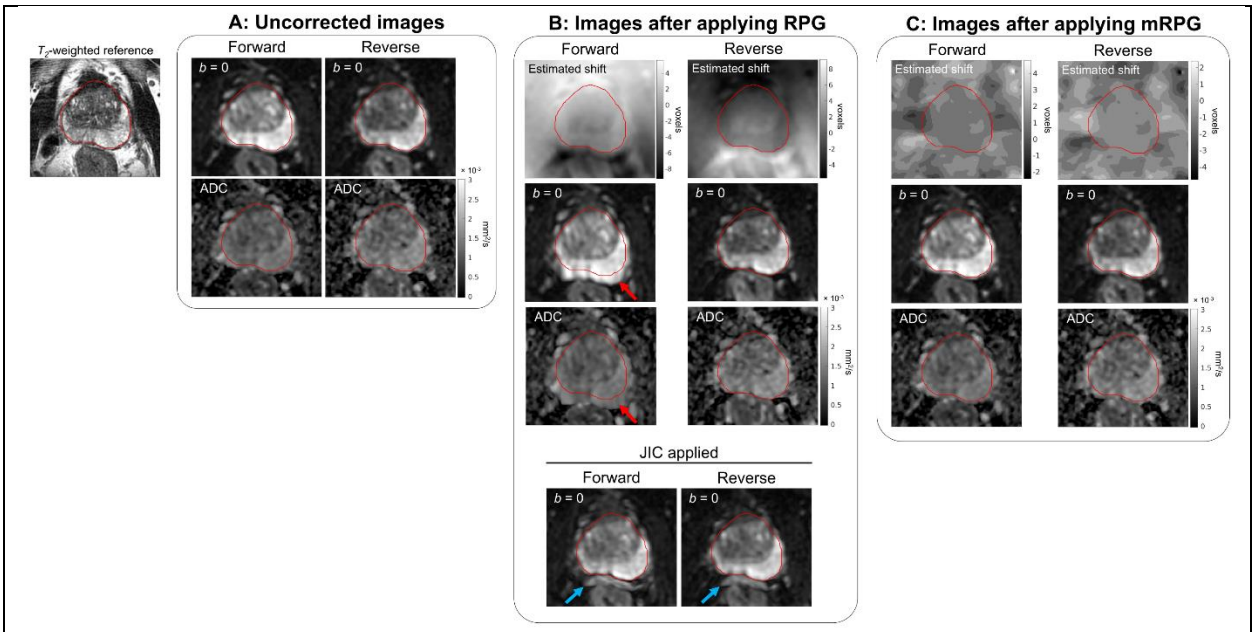

Figure 3: Example of "ghost tissue" created by Jacobian intensity correction (JIC). JIC can result in misleading, false correction of EPI distortion. An undistorted spin echo image is shown (left) with the prostate outlined in red. A) Uncorrected images show minimal EPI distortion. B) RPG incorrectly estimated large shifts in the posterior prostate (red arrows). JIC concealed the erroneous spatial shift while also creating false anatomical structure or "ghost tissue" (blue arrows). mRPG, by contrast, yielded appropriate spatial correction.

Discussion

This study demonstrated a clear disparity in the performance of conventional distortion correction methods when the JIC is applied versus when it is omitted. While RPG and FSL topup yielded large improvements in the correlation between forward and reverse *b*=0 s/mm^2 images, the magnitude of improvement was considerably smaller when the estimated spatial correction was applied without the JIC (obligatory for quantitative ADC maps for which the JIC is meaningless). This disparity suggests an underestimation of the spatial displacement component of EPI distortion, compensated by an overfitting of the signal intensity-scaling component to produce an artificial alignment between forward and reverse volumes.

mRPG circumvents this overfitting problem by removing the intensity scaling (JIC) factor prior to estimating spatial displacement, specifically by normalizing the opposite polarity images across multiple *b*-values. Estimating spatial displacements between the images is then reduced to a simpler image registration problem. As demonstrated in this study, elimination of the JIC component results in significantly improved estimation and removal of spatial distortions compared to conventional RPG or topup.

While mRPG demands additional scan time to acquire multiple *b*-values in both directions, the time cost can be mitigated by acquiring fewer *b*-values than were employed for this study. Recent work has shown that effective distortion correction can be achieved using as few as two *b*-values in either direction (13). Acceleration techniques such as multi-band imaging may also be used. The added scan time required to implement mRPG should also be considered alongside the potential for reduced patient call-back rates and more efficient image interpretation due to mitigation of distortion artifacts.

Improved EPI distortion correction holds significant promise for advancing prostate cancer diagnosis and treatment. Around 70% of prostate cancer lesions occur in the peripheral zone (14, 15), the region of the prostate most likely to be affected by distortion artifacts arising from rectal gas. DWI is also the primary sequence for assessment of peripheral zone lesions according to PI-RADS (1), so EPI distortion artifacts often interfere with radiological diagnosis to a considerable degree. Effective correction of anatomical distortion could therefore enable more accurate diagnosis, biopsy targeting (16) and focal therapy (2) for the majority of clinically encountered lesions. Improved lesion targeting is important for minimizing misdiagnosis or undertreatment of tumor foci, which can impact the chance of tumor recurrence (17, 18). Reduced anatomical distortion could also make it easier for radiologists to distinguish lesions in the prostate from adjacent, benign findings like phleboliths (19), helping to prevent unnecessary targeted biopsies. It may also increase the utility of DWI for evaluating extraprostatic extension, an important prognostic factor (20).

Limitations

Region-of-interest contours were not available for the patients included in this study, precluding a more granular analysis on the impact of distortion correction within different zones or target lesions in the prostate. It would be particularly interesting to examine if distortion correction makes a quantifiable difference in the ADC values within the peripheral zone of the prostate, where EPI distortion artifacts are most pronounced. ADC values are often measured within target lesions, so this analysis could help to quantify the clinical benefit of accurate distortion correction.

Another limitation of this study is that the efficacy of distortion correction was only measured using the correlation between opposite-polarity images. While correlation provides a quantitative measure of the alignment between images, it is not an assessment of diagnostic image quality *per se*. The clinical value of mRPG could be more directly assessed using a reader study, perhaps involving PI-QUAL evaluation (21) by expert radiologists of the images before and after distortion correction.

Conclusion

Conventional distortion correction methods utilizing JIC tend to under-correct (or even exacerbate) anatomical distortions in prostate DWI. Inadequate correction is concealed by application of the JIC, as any misestimation of the true spatial displacement of tissue is compensated by overfitting the signal intensity-scaling component of the correction to produce artificial alignment between opposite-polarity images.

mRPG is proposed as an alternative approach to distortion correction that removes the JIC factor prior to estimating tissue displacement, specifically by normalizing opposite-polarity images across multiple *b*-values. While this approach requires additional scan time to acquire multiple *b*-values for both phase-encoding polarities, it shows significantly improved estimation and removal of spatial distortions compared to conventional methods, and could potentially enable more accurate biopsy targeting and focal therapy of prostate cancer lesions.

References

1. Weinreb JC, Barentsz JO, Choyke PL, et al.: PI-RADS Prostate Imaging – Reporting and Data System: 2015, Version 2. *European Urology* 2016; 69:16–40.

2. Lui AJ, Kallis K, Zhong AY, et al.: ReIGNITE Radiation Therapy Boost: A Prospective, International Study of Radiation Oncologists' Accuracy in Contouring Prostate Tumors for Focal Radiation Therapy Boost on Conventional Magnetic Resonance Imaging Alone or With Assistance of Restriction Spectrum Imaging. *International Journal of Radiation Oncology, Biology, Physics* 2023; 117:1145–1152.

3. Rakow-Penner RA, White NS, Margolis DJA, et al.: Prostate diffusion imaging with distortion correction. *Magnetic Resonance Imaging* 2015; 33:1178–1181.

4. Holland D, Kuperman JM, Dale AM: Efficient correction of inhomogeneous static magnetic field-induced distortion in Echo Planar Imaging. *NeuroImage* 2010; 50:175–183.

5. Andersson JLR, Skare S, Ashburner J: How to correct susceptibility distortions in spin-echo echo-planar images: application to diffusion tensor imaging. *NeuroImage* 2003; 20:870–888.

6. Smith SM, Jenkinson M, Woolrich MW, et al.: Advances in functional and structural MR image analysis and implementation as FSL. *NeuroImage* 2004; 23:S208–S219. [*Mathematics in Brain Imaging*]

7. Conlin CC, Feng CH, Rodriguez-Soto AE, et al.: Improved Characterization of Diffusion in Normal and Cancerous Prostate Tissue Through Optimization of Multicompartmental Signal Models. *Journal of Magnetic Resonance Imaging* 2021; 53:628–639.

8. Feng CH, Conlin CC, Batra K, et al.: Voxel-level Classification of Prostate Cancer on Magnetic Resonance Imaging: Improving Accuracy Using Four-Compartment Restriction Spectrum Imaging. *Journal of Magnetic Resonance Imaging* 2021; 54:975–984.

9. Sunoqrot MRS, Nketiah GA, Selnæs KM, Bathen TF, Elschot M: Automated reference tissue normalization of T2-weighted MR images of the prostate using object recognition. *Magn Reson Mater Phy* 2021; 34:309–321.

10. Jenkinson M, Beckmann CF, Behrens TEJ, Woolrich MW, Smith SM: FSL. *NeuroImage* 2012; 62:782–790. [*20 YEARS OF fMRI*]

11. Hintze JL, Nelson RD: Violin Plots: A Box Plot-Density Trace Synergism. *The American Statistician* 1998; 52:181–184.

12. Hoffmann H: violin.m - Simple violin plot using matlab default kernel density estimation. 2015.

13. Loubrie S, Conlin CC, Batasin SJ, et al.: Multi b-value Reverse Polarity Gradient Distortion Correction for Breast Diffusion-Weighted MRI. In *Proceedings of the International Society for Magnetic Resonance in Medicine*. *Volume 32*; 2024.

14. McNeal JE, Redwine EA, Freiha FS, Stamey TA: Zonal distribution of prostatic adenocarcinoma. Correlation with histologic pattern and direction of spread. *Am J Surg Pathol* 1988; 12:897–906.

15. Yu X, Liu R, Song L, Gao W, Wang X, Zhang Y: Differences in the pathogenetic characteristics of prostate cancer in the transitional and peripheral zones and the possible molecular biological mechanisms. *Front Oncol* 2023; 13.

16. Martin PR, Cool DW, Fenster A, Ward AD: A comparison of prostate tumor targeting strategies using magnetic resonance imaging-targeted, transrectal ultrasound-guided fusion biopsy. *Medical Physics* 2018; 45:1018–1028.

17. Zhong AY, Lui AJ, Kuznetsova S, et al.: Clinical Impact of Contouring Variability for Prostate Cancer Tumor Boost. *International Journal of Radiation Oncology, Biology, Physics* 2023; 117:e455.

18. Zhong AY, Lui AJ, Kuznetsova S, et al.: Clinical Impact of Contouring Variability for Prostate Cancer Tumor Boost. 2024:2024.01.29.24301942.

19. Panebianco V, Giganti F, Kitzing YX, et al.: An update of pitfalls in prostate mpMRI: a practical approach through the lens of PI-RADS v. 2 guidelines. *Insights Imaging* 2017; 9:87–101.

20. Fleshner K, Assel M, Benfante N, et al.: Clinical Findings and Treatment Outcomes in Patients with Extraprostatic Extension Identified on Prostate Biopsy. *J Urol* 2016; 196:703–708.

21. Giganti F, Kirkham A, Kasivisvanathan V, et al.: Understanding PI-QUAL for prostate MRI quality: a practical primer for radiologists. *Insights Imaging* 2021; 12:59.